Journal of Catalysis **201,** 22–36 (2001)
doi:10.1006/jcat.2001.3227, available online at http://www.idealibrary.com on IDEAL®

Ultrasonically Controlled Deposition–Precipitation

Co–Mo HDS Catalysts Deposited on Wide-Pore MCM Material

M. V. Landau,*,[1] L. Vradman,* M. Herskowitz,* Y. Koltypin,† and A. Gedanken†

*Blechner Center for Industrial Catalysis and Process Development, Chemical Engineering Department, Ben-Gurion University of the Negev, Beer-Sheva 84105, Israel; and †Department of Chemistry, Bar-Ilan University, Ramat-Gan 52900, Israel

Received September 14, 2000; revised March 12, 2001; accepted March 12, 2001; published online May 24, 2001

Mo and Co oxides were precipitated under ultrasonication treatment from $Mo(CO)_6$ and $Co(CO)_3NO$ dissolved in decalin. Introduction of wide-pore Al-MCM-41 material with an average pore diameter 8.3 nm and a surface area of 840 m^2/g increased the Mo oxide precipitation rate by an order of magnitude. This is a result of an ultrasonically induced chemical interaction between metal carbonyl (oxide) and the surface silica atomic layer yielding surface silicates (XPS, MAS NMR). It was demonstrated for the first time that ultrasonication of such a slurry yields deposition–precipitation of the corresponding metal oxide, forming a close-packed monolayer at the support's surface (N_2 adsorption, HR-TEM, XPS, XRD). Ultrasonically controlled deposition–precipitation produced ~45 wt% MoO_3 loading, which is saturation of the wide-pore Al-MCM-41 surface monolayer. The high-loading Co–Mo/Al-MCM-41 catalyst prepared by ultrasonically controlled deposition–precipitation was 1.7 times more active in HDS of dibenzothiophene, based on the reaction rate normalized per catalyst weight, than commercial Co–Mo–Al catalyst.

Key Words: **catalyst preparation by ultrasonication; deposition–precipitation; Co–Mo on MCM-41; Mo oxide monolayer; HDS.**

1. INTRODUCTION

MCM materials (1), mesoporous silicas or alumina silicas with ordered nanotubular pores, have a significantly higher surface area (700–1500 m^2/g) than conventional catalyst supports such as silica gels, aluminas, and alumina silicates. This property is especially important for "active-phase-support" type solid catalysts that require stabilization of the phase (phases) of active components at high dispersion level. In low-percentage catalysts, like Pt/SiO_2 (3, 4), Ni/SiO_2 (5), or CrO_2/SiO_2 (6), that contain <5 wt% active phase deposited on conventional silica gels (300–400 m^2/g), close to 100% dispersion can be accomplished due to the low surface concentration of the active component. Since the surface properties of MCM are similar to those of amorphous silica gels or alumina silicas (2), the advantage of using MCM materials could be expected in the preparation of high-percentage catalysts with relatively high dispersion. High-loading catalysts are widely used in various important commercial processes, such as hydrotreating of oil fractions (Co(Ni)–Mo(W)), hydrogenation (Ni–, Cu–Zn–, Cu–Cr–), dehydrogenation (CrO_3–), and others.

However, taking full advantage of MCM supports in preparation of improved catalysts requires molecular (atomic) dispersion of the active-phase precursor at the deposition stage. Several attempts were made to prepare Co(Ni)–Mo sulfide hydrotreating catalysts by sulfidation of Co(Ni)–Mo oxide precursors deposited on MCM supports by impregnation (7, 8) or thermal spreading (9, 10). The performance of those catalysts in hydrodesulfurization (HDS) of oil fractions or model compounds was poor compared with that of modern Co(Ni)–Mo–Al commercial catalysts. Poor dispersion of the active phase, due to the relatively low dispersion of sulfide-phase precursors in the absence of chemical interaction with support surface, was one problem. Significant pore blocking even at relatively low loading of active components (up to about 15 wt%) was another.

High dispersion of Co(Ni)–Mo(W) precursors on the silica surface could be achieved by ion-exchange with silanols modified at high pH (Co, Ni) or anchoring–grafting of coordinative metal compounds (Mo, W) by surface silanols. Catalysts with high specific activity such as Ni–W and Ni–Mo sulfide supported on silica gel were prepared at the comparatively low Mo(W) loading of <8 wt% (11, 12). Preparation of high-loading catalysts using those methods that require specific interaction between metal precursor and surface silanols is limited by the surface concentration of the silanols. The silanols' concentration in MCM materials is about 2 times lower than that in silica gels (13). This limitation could be overcome by using the "homogeneous deposition–precipitation" (HDP) method developed by Geus and co-workers (14, 15).

The HDP method includes two stages: conversion of highly soluble substance A (a precursor of active

[1] To whom correspondence should be addressed. Fax: 972-8-6477678. E-mail: mlandau@bgumail.bgu.ac.il.

0021-9517/01 $35.00

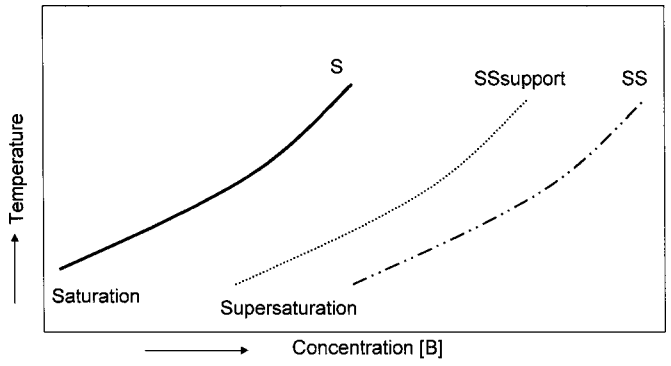

FIG. 1. Phase diagram.

component) to a precursor B_L with low solubility followed by physical or chemically induced precipitation to B_S. The conversion of A in the first stage requires an additional controlling component like a base (provided directly (14, 15) or by means of voltage for electrochemical reactions (16)) or a reducing agent (17). The level of the controlling component determines the extent of conversion. At a given B_L concentration and temperature, the precipitation stage 2 proceeds if B_L reaches a supersaturation level marked as SS in Fig. 1. Insertion of a support that provides nonspecific interaction of the surface with precursor B_L decreases the precipitation barrier of B_L to B_S from SS to $SS_{support}$. Therefore, between the SS and $SS_{support}$ curves, precursor B_L is converted to precursor B_S only on the support surface, excluding precipitation in the bulk liquid.

The HDP of Mo and Co oxides on the MCM surface requires a suitable precursor A and proper conditions for conversion to B_L: the controlling component and its level. Dhas and Gedanken reported (18, 19) that ultrasonication of $Mo(CO)_6$ solution in decalin containing nonporous silica microspheres yielded Mo–silica composites. According to TEM micrographs, particles of Mo oxide phase were located mostly on the silica surface. This means that $Mo(CO)_6$ undergoes decomposition–oxidation with dissolved oxygen to Mo oxide under intensive ultrasonication. It could be used for Mo oxide HDP on MCM materials as reaction $A \rightarrow B_L$, where ultrasonication energy is the controlling component in this reaction. No information about sonochemical deposition of Co oxide on silica was found. It is known that Co oxide could be obtained by thermal decomposition of Co hydroxide precipitated from $Co(CO)_3NO$ solutions under ultrasonication (20).

This study was aimed at exploring the ultrasonically controlled HDP method. Novel preparation of high-loading Co–Mo–MCM catalysts, characterization, and testing of their performance in dibenzothiophene HDS in comparison with a commercial Co–Mo–Al catalyst will be presented.

2. EXPERIMENTAL

2.1. Catalysts Preparation

Two supports, commercial γ-alumina and Al-MCM-41, with similar average pore diameter in the range 8–10 nm, were used in this study. This pore range is optimal in the preparation of commercial Co–Mo–Al catalysts for hydrotreating of middle distillates, minimizing the internal diffusion limitations. Their texture characteristics derived from nitrogen adsorption–desorption isotherms are shown in Table 1.

γ-Alumina was purchased from Norton Co. (SA 6175). The wide-pore Al-MCM-41 material was prepared according to a modified method (1) using mesitylene as solubilization agent for cetyltrimethylammonium chloride (CTAC) surfactant micelles. Crystallization was performed from a gel composition: 1.0 SiO_2 : 0.04 Al_2O_3 : 0.26 CTAC : 2.6 mesitylene : 0.04 Na_2O : 21.2 H_2O. A 75 g amount of mesitylene (Aldrich) was added to 80 g of a 25% aqueous solution of CTAC (Aldrich) at room temperature. A 1.65 g amount of sodium aluminate powder was added to this mixture under vigorous stirring (the sodium aluminate was synthesized by reaction of equimolar amounts of aluminum hydroxide (bohemite) and NaOH followed by drying and calcination at 550°C). A 40 g amount of a 20% aqueous solution of tetramethylammonium silicate (Aldrich) was added dropwise to this mixture under stirring. Next 10 g of powdered silica (Hisil, Degussa) was added in small portions. The final mixture was stirred for 15 min at room temperature. The gel was crystallized in a Teflon-coated autoclave at 105°C under stirring (100 rpm) for 4 h. The solid was separated by filtration, washed with 500 ml of distilled water on the filter, and dried in air at room temperature for 16 h. Additional drying at 100°C for 4 h and calcination at 500°C for 4 h, raising the temperature at 1°C/h, completed the preparation. The Al_2O_3 content was 0.9 wt%. No ion-exchange for sodium removal was carried out; thus, the main role of Al is stabilization of wide-pore Al-MCM-41 hexagonal structure. Without addition of this minimal amount of sodium aluminate, the pure silica wide-pore MCM-41 could not be synthesized by the selected procedure due to its low thermal stability.

The impregnation of both supports with aqueous solution containing Co and Mo compounds was carried out

TABLE 1

Texture of Supports

Support	Surface area (m^2/g)	Pore volume (cm^3/g)	Average pore diameter[a] (nm)
γ-Alumina	270	0.65	9.6
Al-MCM-41	840	1.74	8.3

[a] Average pore diameter = (4 × pore volume)/(surface area).

according to a procedure described in (21). A 5.56 g amount of $CoCO_3$ (Aldrich) and 1.8 g of aqueous phosphoric acid (85%) were added to 30 ml of water at 40°C. The temperature was increased to 60°C and kept for 1 h. Next, 10.96 g of MoO_3 (Aldrich) was added. The temperature was further increased to 96°C and kept for 2 h. A 4 ml amount of aqueous nitric acid (65%) was added. The solution was diluted with water to the desired concentration (which allows the metal phase content to be controlled in the catalyst) and cooled to room temperature. The incipient wetness method was employed for impregnation. The impregnated material was dried for 1.5 h under vacuum in a rotary evaporator at 95°C, then for 16 h at 120°C in an oven under ambient air, followed by calcination for 2 h at 530°C.

The ultrasonically controlled HDP of Co and Mo oxides was conducted in a slurry of Al-MCM-41 or γ-alumina in 120 ml of decalin solution containing dissolved $Mo(CO)_6$ and/or $Co(CO)_3NO$. The sonication was carried out by employing a high-intensity Ti-horn (20 kHz, 100 W/cm^2) sonicator under ambient air at room temperature for periods of up to 4 h. The solid product was separated by centrifugation, thoroughly washed with dry pentane, and dried in a vacuum at room temperature.

Bulk molybdenum oxide (blue oxide) was prepared by sonication of the $Mo(CO)_6$ solution in decalin in the absence of support. Commercial Co–Mo–Al catalyst KF-752 (Akzo Nobel Chemicals) was used as a reference sample in testing experiments. The commercial catalyst and catalysts prepared by Co–Mo deposition on commercial γ-alumina were used in their actual shape and size (1.3-mm extrudates). Pelletization of powdered Co–Mo catalysts deposited on Al-MCM-41 involved pressing and crushing followed by separation of a fraction with an average pellet diameter of 1.3 mm.

2.2. Catalysts Characterization

The chemical composition of solid catalysts (wt%, average of five measurements at different points of the solid) was measured by the SEM-EDAX method (JEM-35 microscope, JEOL Co., link system ANB-1000, Si–Li detector). Surface areas, pore volumes, and pore size distributions were obtained from N_2 adsorption–desorption isotherms using the conventional BET and BJH methods. The samples were outgassed under a vacuum at 250°C. Isotherms were measured at liquid nitrogen temperature with a NOVA-1000 (Quantachrome, Version 5.01) instrument.

Wide-angle XRD patterns were collected on a Phillips diffractometer PW 1050/70 (Cu $K\alpha$ radiation) with a graphite monochromator. The data were recorded with a 0.02° step size, 2 s at every step. The MoO_3 crystal domain size was determined using the Scherrer equation, $K\lambda/[(B^2-\beta^2)^{0.5}\cos(2\theta/2)]$, where $K = 1.000$, $\lambda = 0.154$ nm, and B is the (111) reflection broadening at $2\theta = 33.7°$. The content of the MoO_3 crystalline phase in MCM-supported catalysts was calculated on the basis of the integral intensities of the (020) reflection ($2\theta = 12.8°$) compared with a calibration curve recorded with a series of mechanical mixtures of 1–30 wt% crystalline MoO_3/Al-MCM-41.

The high-resolution TEM (HR-TEM) micrographs were recorded using a JEM 2010 microscope operated at 200 kV and equipped with linked EDS. EDAX was performed in STEM mode to obtain the Mo and Si contents in the sample primary particles at a spot size of 15–25 nm. The samples for HR-TEM were prepared by depositing a drop of an ultrasonicated ethanol suspension of solid catalyst on a carbon-coated Cu grid. The grid was dried at 80°C and mounted on a specimen holder. Samples were examined as grain mounts. Images from thin sample edges were recorded under various focus conditions looking for optimal defocus that allowed clear resolution of hexagonal tubular pores and pore walls of high density to be obtained.

PHI 549 SAM/AES/XPS ultra-high-vacuum (10^{-9} Torr) apparatus with a double cylindrical mirror analyzer (CMA) and a Mg $K\alpha$ (1253.6 eV) X-ray source was used for recording the XPS spectra. After the general survey spectra were recorded, high-resolution scans were taken at pass energy (25 eV) for the major peaks: C 1*s*, Mo 3*d*, Si 2*p*, and O 1*s*. Quantitative analysis was based on published empirical atomic sensitivity factors (22). The spectral components of Mo, Si, and O signals were found by fitting the sum of single-component lines to the experimental data by means of nonlinear least-squares curve-fitting. The single-component line was assumed to have the shape of a sum of Cauchy and Gauss distributions with a maximum at X_0 (the binding energy of the component), peak width parameter (w), the Cauchy–Gauss ratio (m), and the maximum intensity (I) (23).

^{29}Si and ^{1}H magic angle spinning (MAS) NMR experiments were performed on a Bruker DSX-300 spectrometer. All signals were accumulated while the samples were spinning at the magic angle with a spinning frequency of 5 kHz. The sample rotors had a diameter of 4 mm and the spinning stability was less than 5 Hz. ^{29}Si NMR spectra were obtained after Fourier transformation of accumulated echo signals that were collected by a two-pulse echo sequence, (t_p–τ–$2t_p$–τ–*acquisition*), with a 90° pulse length of $t_p = 5\ \mu s$ and a delay time of $\tau = 200\ \mu s$. Additional ^{29}Si NMR spectra were obtained by ^{1}H–^{29}Si cross-polarization CPMAS experiments. The CP contact time was 4 ms and the radio frequency intensity on ^{29}Si equaled 50 kHz. The repetition time of all experiments was 30 s. Free induction decay ^{1}H MAS NMR signals were acquired after a single 90° excitation pulse of 2 μs.

The FTIR spectra were recorded on a Nicolet (Impact 4) spectrometer. The measurements were performed using a KBr pellet. No peaks in the region of 2000 cm^{-1} of the C–O stretching vibrational mode were detected as precipitates of $Mo(CO)_6$ and/or $Co(CO)_3NO$ into Al-MCM-41 or γ-alumina supports. This is an indication that the precursor is not deposited on the surface of the supports.

2.3. Catalysts Testing

The dibenzothiophene (DBT) hydrodesulfurization (HDS) measurements were carried out in a high-pressure, fixed-bed reactor minipilot unit, controlled automatically by a PC that was described in detail elsewhere (24). A 5 cm^3 amount of catalyst mixed with 10 cm^3 of 0.2-mm silicon carbide particles (Norton Co.) was packed in a 12-mm-i.d. stainless steel tubular reactor between two 10-cm layers of 0.2-mm-diameter silicon carbide particles.

All catalysts before HDS measurements were sulfided for 24 h with a 1.5% dimethyl disulfide–toluene mixture at LHSV = 2.5 h^{-1}, 320°C, hydrogen pressure of 3.1 MPa, and H_2/toluene ratio 500 NL/L. The DBT HDS was carried out with 1 wt% DBT dissolved in a 50 wt% *n*-decane–50 wt% *n*-octadecane mixture at 320°C, hydrogen pressure 3.1 MPa, and H_2/liquid ratio of 500 NL/L. The HDS products were analyzed by the GC method using a Chrompack 9001 instrument equipped with a flame ionization detector and a CP-Sil5 CB capillary column, 10 m long with 0.255 mm i.d. No sulfur-containing products other than unconverted DBT were detected; under the selected conditions DBT was converted to biphenyl and cyclohexylbenzene. Therefore, DBT conversion was calculated on the basis of the detected concentration of residual DBT in HDS products.

LHSV varied in the range 40–120 h^{-1}. The DBT conversion (x) for each catalyst was measured as a function of LHSV. DBT conversion was proportional to the space time at $x < 50\%$. This pseudo-zero-order HDS kinetics is generally observed at high DBT concentrations (~1 wt%) due to the self-inhibition effect (25, 26). The pseudo-zero-order DBT HDS rate constant normalized per catalyst weight was calculated according to the equation

$$k_w = x(\mathrm{LHSV})/\rho_b, \qquad [1]$$

where $k_w = k/C_0$ (C_0 is the inlet DBT concentration, k is the pseudo-zero-order HDS rate constant) and ρ_b is the catalyst's bulk density. In addition, the DBT HDS rate was calculated as the turnover number, TON (h^{-1}), defined as the amount of reacted DBT molecules per hour normalized per number of Mo atoms loaded in the reactor with the catalyst sample. The TON characterizes the HDS efficiency of the Mo phase promoted with cobalt (Co–Mo–S) since the Co phase itself is almost inactive in HDS (27, 28).

3. RESULTS AND DISCUSSION

3.1. HDP of Mo and Co Oxide Phases

The Mo deposition kinetics was measured by determining the amount of precipitate and analyzing the Mo concentration in precipitate probes taken at time periods after sonication of the $Mo(CO)_6$ solution in the presence and in the absence of Al-MCM-41. According to FTIR spectra the precipitates did not contain $Mo(CO)_6$ species: no bands at 2000 cm^{-1} characteristic of the C–O stretching vibration were detected. According to XPS data, the deposited Mo/Al-MCM-41 samples contained the same amount of carbon as the pure Al-MCM-41 sample, which corresponded to adsorbed carbon (binding energy 284.6 eV) (29). No other carbon peaks were detected. This is evident for no Mo carbide formation. XRD patterns of precipitated samples did not contain clear peaks due to their amorphous character. It means that ultrasonication in both cases caused deposition of amorphous Mo oxide formed as a result of $Mo(CO)_6$ decomposition–oxidation in the presence of atmospheric air as was proved in (18, 19), forming Mo oxide of very low solubility.

Under ultrasonication of $Mo(CO)_6$ in decalin solution with a starting concentration of 4.75 g of $Mo(CO)_6$/L, the amount of deposited Mo oxide phase (calculated as MoO_3 from EDAX data) increased with time in the presence and in the absence of Al-MCM-41 support (Fig. 2a). Addition of support at 2.5 g of Al-MCM-41/L concentration drastically increased the Mo carbonyl decomposition–precipitation rate. Approximation of the Mo deposition rate by pseudo-first-order kinetics relative to the Mo carbonyl concentration yielded a decomposition–precipitation rate increase by a factor of more than 7 after insertion of Al-MCM-41 (Fig. 2b).

The $Mo(CO)_6$ concentration in decalin was changed at fixed Al-MCM-41 loading to control the concentration of the Mo oxide phase in the precipitate (Fig. 3). The slurry was sonicated in every case for 4 h at an Al-MCM-41 concentration of 5 g/L. In all the experiments, the Mo oxide content in the precipitates corresponded to about 67% conversion of $Mo(CO)_6$ (Fig. 3). This is in good agreement with deposition kinetic data fit by first order relative to $Mo(CO)_6$ concentration. Indeed, only for first-order kinetics, the conversion is not dependent on the Mo carbonyl concentration, so the rate constant at a fixed Al-MCM-41 content is a function of ultrasonication intensity (constant in all the experiments).

The significant increase of the Mo oxide deposition rate after insertion of Al-MCM-41 support supposes a strong interaction between the support and Mo oxide (Mo carbonyl). This interaction is induced by ultrasonication since attempts to deposit Mo or Co oxides onto Al-MCM-41 by the same procedure without sonication were unsuccessful. Neither Mo nor Co (EDAX) nor Mo (Co) carbonyls (FTIR) were detected in the product without sonication treatment; the carbonyls were washed out from MCM pores by pentane. The ultrasonically induced chemical interaction between Mo precursor (carbonyl or oxide) and Al-MCM-41 support should yield new silicate-type compounds with characteristic chemical state of Mo, Si, and O atoms. This was demonstrated from the binding energy of characteristic

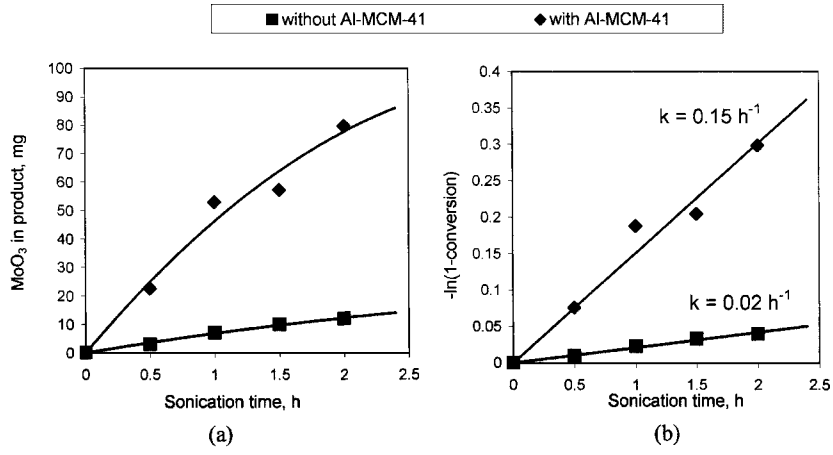

FIG. 2. Kinetics of MoO_x formation under ultrasonication of $Mo(CO)_6$ solution.

electrons measured by XPS for pure Al-MCM-41, for Mo oxide precipitated under sonication in the absence of Al-MCM-41, and for MoO_x–Al-MCM-41 composites obtained by ultrasonically controlled deposition.

The XPS spectra of Si 2*p*, O l*s*, and Mo 3*d* core levels in those samples are shown in Fig. 4. Mo deposition created a new band in the Si 2*p* spectra at a binding energy 102.2 eV in addition to the band at 103.4 eV characteristic of Si atoms in silica gels (29) (Fig. 4a). The intensity of this new band strongly increased with increasing Mo loading in ultrasonically deposited sample from 21 to 56 wt%. According to (29), bands with binding energy of 102.5 eV in XPS spectra are characteristic of the state of silicon atoms in silicate anions. In XPS spectra of O 1*s* core level, two additional bands at binding energies of 531.2 and 530.1 eV were detected besides oxygen with a binding energy of 532.8 eV, characteristic of Al-MCM-41 support. Their intensity increased with the increase of Mo loading (Fig. 4b). One of these new bands, with a binding energy of 530.1 eV, corresponded to O 1*s* in amorphous Mo oxide precipitated by ultrasonication in the absence of Al-MCM-41. It could be attributed to terminal double-bonded oxygen atoms in Mo oxide. Another band (531.2 eV) could be related to bridged Si–O–Mo oxygen formed from an ultrasonically induced Mo oxide–support interaction. Minor differences were detected in the XPS spectra of the Mo 3*d* core: broadening of bands at binding energies of 236 and 232.7 eV in MoO_x/Al-MCM-41 composites compared with ultrasonically deposited pure MoO_x (Fig. 4c). The XPS data confirm the ultrasonically induced chemical interaction between Mo oxide and the silica

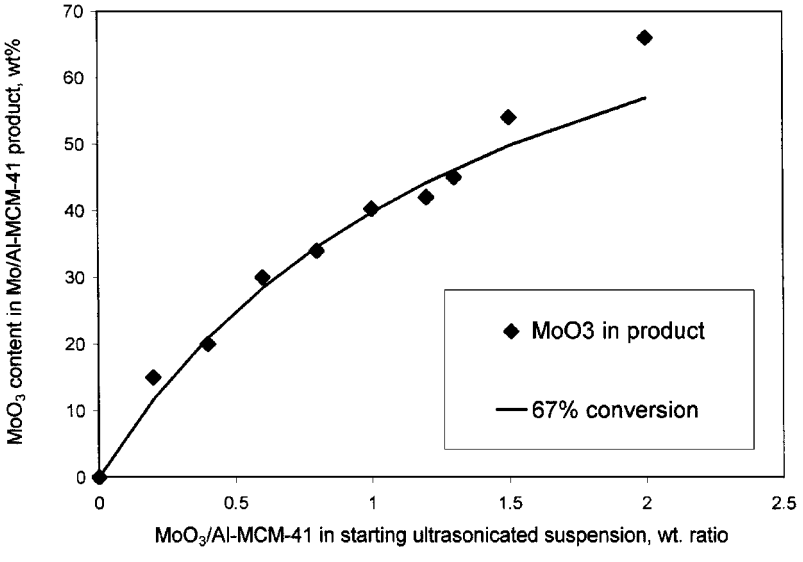

FIG. 3. Effect of Mo-carbonyl concentration in slurry on amount of MoO_x deposited on Al-MCM-41.

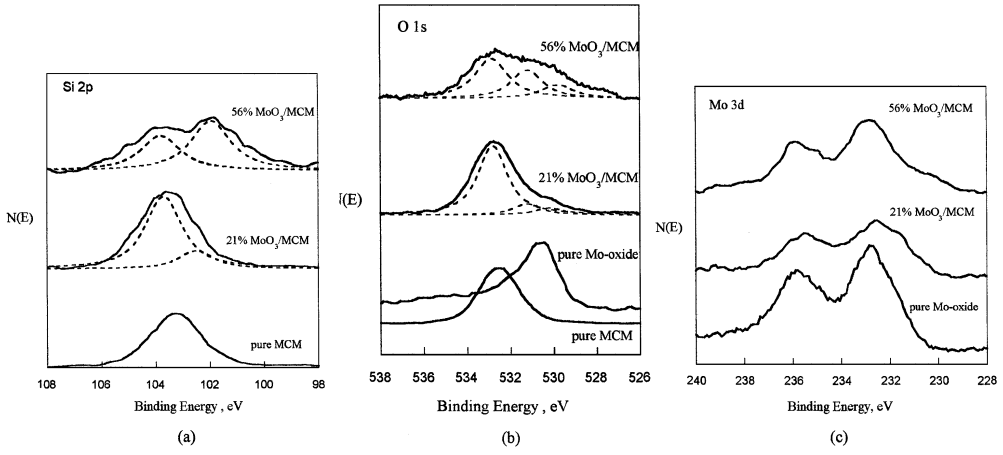

FIG. 4. XPS spectra of MoO_x/Al-MCM-41 samples prepared by ultrasonically controlled HDP.

surface, forming surface silicate species, detected first in (19) using nonporous silica.

The driving force of this interaction is insertion of acoustic energy into the reacting system. The chemical consequences of high-intensity ultrasound do not arise from an interaction of acoustic waves and matter at a molecular and atomic level. Instead, in liquids irradiated with high-intensity ultrasound, acoustic cavitation (the formation, growth, and collapse of bubbles) provides the primary mechanism for sonochemical effects. Bubble collapse produces extremely high temperatures (~5000°C) and pressures (~1000 atm) and very high heating and cooling rates (~10^{10} K/s). Thus, cavitation serves as a means of concentrating the diffuse energy of sound into a unique set of conditions to produce unusual materials from dissolved (and generally volatile) precursors (30). It is clear that the bubble cannot collapse inside the mesopores because the size that the bubble reaches before its collapse is estimated at about 100 μm (30). But cavitation near the liquid–solid interface is very different from cavitation in liquids (31). Near a solid surface, the collapse drives high-speed jets of liquid and shock waves. Since most of the energy is transferred to the accelerating jet, the jet can reach velocities of hundreds of meters per second. In our case, the small hydrated MoO_x clusters produced by cavity collapse (18, 19) in the vicinity of the external surface of primary Al-MCM-41 crystals or their agglomerates are pushed into mesopores by highly turbulent mixing and, due to their reaction with the surface oxygen atoms (of silanols or siloxane bridges), are anchored to the inner surface of the support. Upon this interaction the $MoOx \cdot nH_2O$ clusters produced by cavity collapse overcome breakdown and partial dehydration. This leads to formation of monomeric MoO_x–surface complexes (32) resembling the well-known thermal spreading of Mo oxide onto silica supports (32, 33). In addition, shock waves created by cavity collapse may also induce surface damage (e.g., breaking of siloxane bridges (19)), which can accelerate the chemical interactions between the support and the Mo-phase precursor.

The ^{29}Si and ^{1}H MAS NMR spectra of the parent Al-MCM-41 support and the 45 wt% MoO_3/Al-MCM-41 composite sample prepared by ultrasonically controlled HDP are shown in Fig. 5. No significant differences could be observed between the ^{29}Si echo signals. This indicates that the majority of silicon atoms in the two samples are equally coordinated in terms of distribution of sites with equal chemical shifts. Therefore, no changes in the bulk structure of the interporous walls after formation of the compact Mo oxide monolayer were recorded. It does not exclude formation of Mo–O–Si bonds in [MoO–SiO_3] units assuming that they have the same chemical shifts as the Q^3 [OH–SiO_3] or strained Q^4 [SiO_4] units at the supports surface. This is true even if the local structure of Si in the Al-MCM-41 starting material would not resemble in any conceivable way the local structure of Si in Si–O–Mo species. It is in agreement with the data reported recently by Piquemal *et al.* (34) where no new signals besides that corresponding to Q^2, Q^3, and Q^4 silica units in pure silica MCM-41 and no differences in the relative intensities of these signals were detected in mesoporous molybdosilicate with MoO_3 content ~7 wt%. Si–O–Mo species were prepared in (34) by special chemical routes leading to isomorphous substitution of silicon atoms for molybdenum inside the pore walls of hexagonal MCM-41 material.

The ^{29}Si CPMAS spectra of the parent Al-MCM-41 and 45 wt% MoO_3/Al-MCM-41 samples in Fig. 5 (central column) are drawn on the same scale as their corresponding echo signals (left column in Fig. 5). Thus their intensities correspond to the same total number of ^{29}Si atoms in the sample and can be compared quantitatively. From these spectra it follows that deposition of the Mo oxide monolayer increases the amount of internal surface protons—^{29}Si with nearby hydroxyls. The relative intensities of the silicon atoms in sites Q^3 and Q^4 differ from the intensities

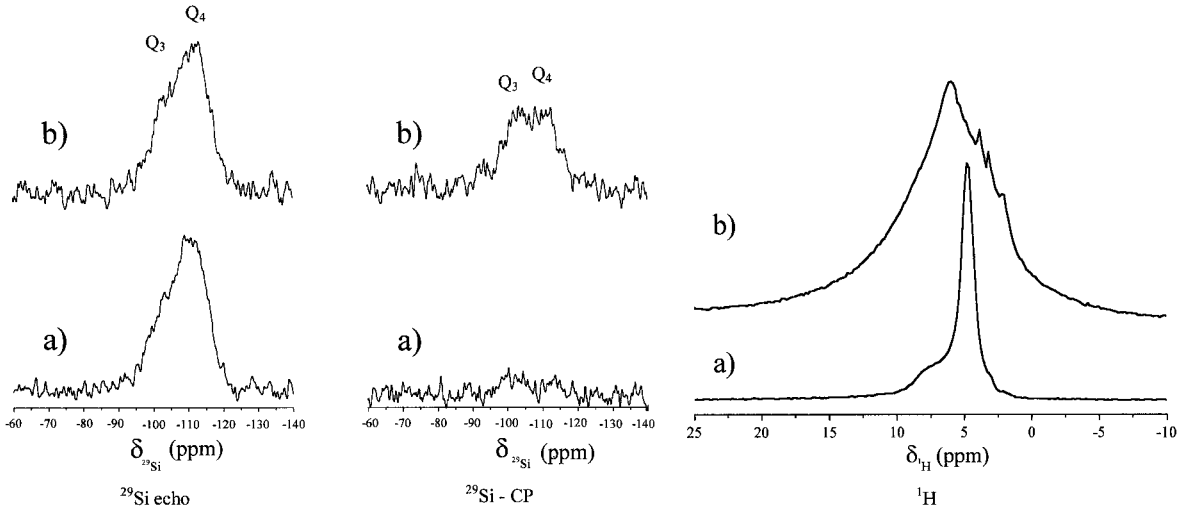

FIG. 5. ^{29}Si and ^{1}H NMR spectra of parent Al-MCM-41 material (a) and 45% MoO_3/Al-MCM-41 composite (b) obtained by ultrasonically controlled HDP.

in echo signals, indicating that as expected Q^3 sites are located closer to the surface than Q^4 sites. To verify the increase in the amount of surface protons by Mo oxide deposition, ^{1}H MAS spectra of the two samples (right column in Fig. 5) were collected. The ^{1}H MAS spectrum of Al-MCM-41 shows two lines that can be assigned to water (broad base line) and protons of surface silanols (sharp peak). They are of about equal integral intensity. This changes drastically in the ^{1}H MAS spectrum of Al-MCM-41 containing deposited Mo oxide. Here almost all protons originate from water molecules, and a very small relative concentration of silanols remained after Mo oxide deposition. The three small lines between 4 and 2 ppm could be correlated to protons of OH groups formed as a result of hydrated Mo oxide deposition and connected with surface MoO_x sites.

The XPS and MAS NMR data are evidence for chemical interaction between the Al-MCM-41 surface and $Mo(CO)_6$ in decalin under ultrasonication as shown schematically in Fig. 6. As was shown in (18, 19), the sonolysis of $Mo(CO)_6$ in decalin containing dissolved oxygen leads to deposition of hydrated Mo oxide as a result of a decomposition–oxidation reaction:

$$2Mo(CO)_6 + 9.5O_2 \xrightarrow{\text{decalin}} Mo_2O_5 \cdot 2H_2O + 12CO_2. \quad [2]$$

In this reaction, decalin is a source of protons for formation of water molecules in solvated Mo oxide. In the presence of Al-MCM-41, the reaction of its surface silanols with unsaturated MoO_x species substantially accelerates the sonolysis of $Mo(CO)_6$ at the support surface. This yields hydrated MoO_x species anchored to the Al-MCM-41 surface by Mo–O–Si bridges in full agreement with XPS and MAS NMR data. The fact that the anchored species are hydrated could explain the increasing density of surface protons—^{29}Si with nearby hydroxyls, detected by NMR. Indeed, formation of a Mo phase monolayer caused the replacement of almost all the protons of the surface silanols (right column in Fig. 5), but since this monolayer consists of hydrated species it introduces more protons that originated from water molecules. In addition, the increasing density of surface protons in close vicinity of ^{29}Si relative to parent Al-MCM-41 implies a high surface concentration of anchored hydrated MoO_x species—much higher than the concentration of silanols in parent Al-MCM-41. Thus, it could be assumed that ultrasonication also promotes the splitting of surface siloxane bridges in strained Q^4 units (Fig. 6) that arise at the surface of MCM-41 material after removal of the surfactant molecules (35). This assumption explains the high capacity of the Al-MCM-41 surface to anchore MoO_x species despite the relatively low silanols concentration, up to formation of close-packed monolayer (as will be shown below).

The strong increase of the ultrasonically controlled Mo oxide deposition rate in the presence of Al-MCM-41,

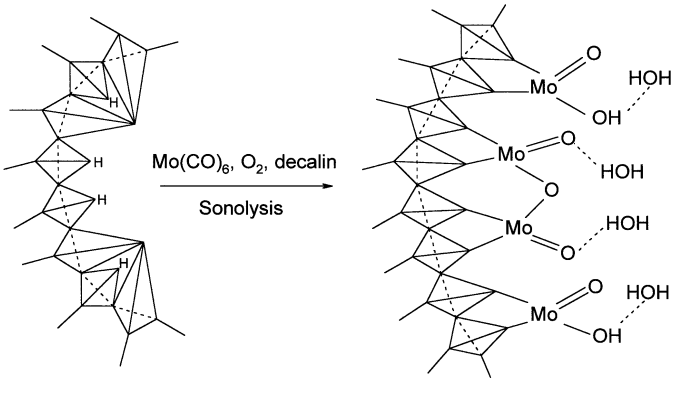

FIG. 6. Scheme of sonolysis of $Mo(CO)_6$ at the Al-MCM-41 surface.

detected in kinetic experiments (Fig. 2), could be explained by Mo precursor–support interaction. Since formation (precipitation) of Mo oxide under the selected conditions occurred also in the absence of support, the concentration of Mo oxide (B_L) formed by $Mo(CO)_6$ decomposition–oxidation is higher relative to the $(B_L)_{SS}$ curve (Fig. 1). The nonspecific Mo precursor–Al-MCM-41 chemical interaction, detected by XPS, enhances the Mo deposition that could be expressed by shifting the supersaturation (SS) curve in Fig. 1 to lower B_L concentrations ($SS_{support}$) in the presence of the Al-MCM-41 support.

The second Co component was deposited onto Al-MCM-41 under ultrasonication from $Co(CO)_3NO$ solution in decalin by two methods:

(1) Ultrasonically controlled codeposition with Mo oxide after dissolution of both carbonyls in the same amount of solvent.

(2) Two-step deposition where dried MoO_x/Al-MCM-41 was inserted into $Co(CO)_3NO$ in decalin solution and sonicated under the same conditions.

The ultrasonication in one- or two-step deposition experiments was done for 4 h. As with the pure Mo component, in both cases no cobalt carbonyl, nitrate, or carbide was detected in Co-Mo/Al-MCM-41 deposited samples.

The codeposition method displayed poor reproducibility of Co and Mo loading in Co–Mo Al-MCM-41 composites (Fig. 7a). After sonication under the same conditions and the same starting Co/support and Mo/support ratios, the final Co and Mo oxide loading varied in the range of 7–10 wt%. This could be a result of competition between Co and Mo oxide species interacting with the silica surface and interaction between Co and Mo precursors in solution. The two-step deposition gave good reproducibility of Co loading that could be well controlled, as in the case of Mo,

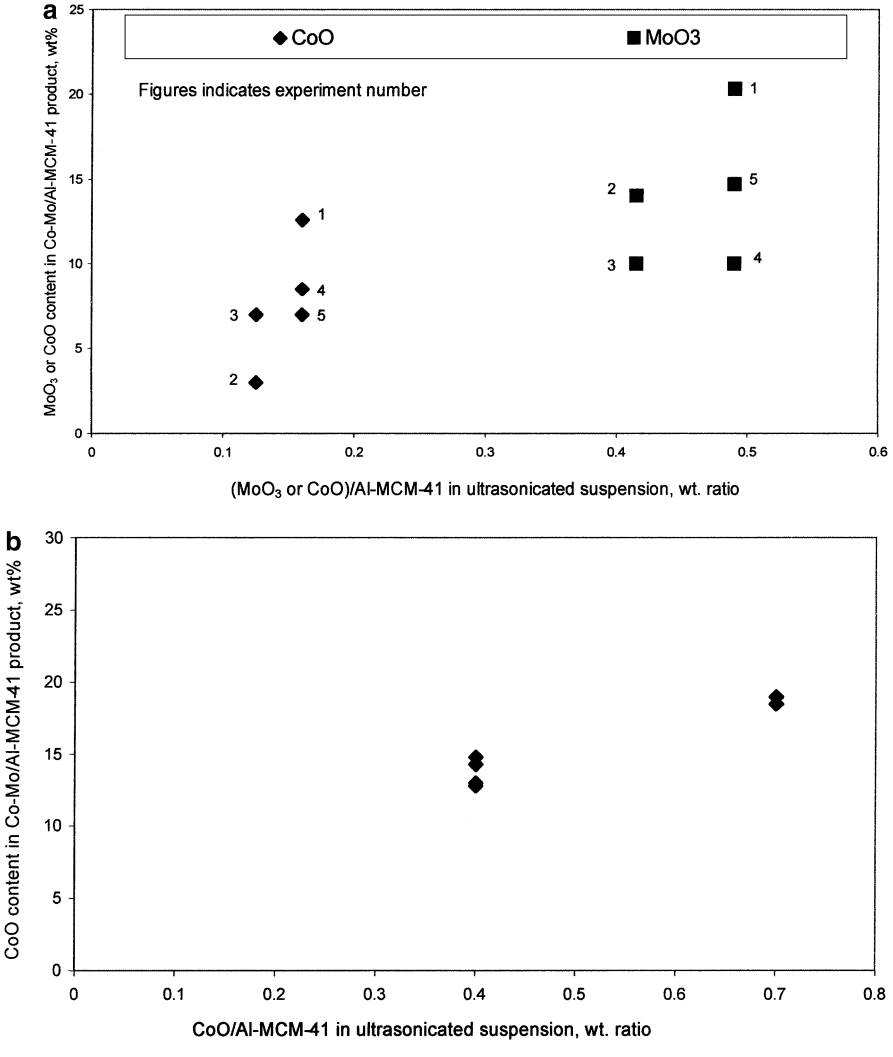

FIG. 7. Effect of $Mo(CO)_6$ and $Co(CO)_3NO$ concentration in slurry on amount of metal oxides deposited on Al-MCM-41: (a) Mo and Co oxides codeposition; (b) Co oxide deposition on 50% MoO_3/Al-MCM-41.

by varying the starting Co/support ratio (Fig. 7b). It seems that the deposition of Mo oxide strengthens the interaction of support with the Co precursor due to formation of an XRD-amorphous mixed Co–Mo oxide phase.

Ultrasonically controlled HDP of Co–Mo oxides onto a commercial γ-alumina support was done by the two-step method under the same conditions as with Al-MCM-41. The Co and Mo loading were well controlled by the Co/support and Mo/support ratios in the starting slurry.

3.2. Location and Dispersion of Mo(Co) Active Phase

3.2.1. TEM and HR-TEM measurements. Since Mo oxide is precipitated by ultrasonication from $Mo(CO)_6$ solution under the selected conditions in the absence of Al-MCM-41 support, at least part of it could exist in the MoO_x/support composite in the form of separate particles outside of the support pores. TEM-EDAX was employed to measure the chemical composition of selected primary particles observed in TEM images of composite samples. The TEM micrographs of pure Al-MCM-41 and three MoO_x/Al-MCM-41 composites obtained by ultrasonically controlled HDP at different Mo/support ratios are shown in Fig. 8. The composites consisted of friable aggregates of Al-MCM-41 crystals and close to globular shape 50–200-nm particles of the MoO_x phase. At low Mo content (21 wt% MoO_3, Fig. 8b) no globular MoO_x particles were detected (looking at the 15 different 85×85 μm^2 areas of the sample), the sample's morphology was close to that of parent Al-MCM-41 (Fig. 8a). All the EDAX data collected with an electronic spot 25 nm from the different points of friable aggregates shown in Fig. 8b gave similar MoO_3 contents (average of 10 measurements) compared with the averaged composition measured by SEM-EDAX. The same result was obtained with composite containing 45 wt% MoO_3. Only one ~200-nm globular particles agglomerate with >90 wt% MoO_3 content (labeled by white arrow, Fig. 8c) was found in this sample. At a MoO_3 content of 66 wt%, many separate globular 40–60-nm particles of pure MoO_x phase (labeled by white arrows, Fig. 8d) were observed. In this case, the MoO_3 content in the Si-containing friable aggregates was 10–20% lower compared with the average composition measured by SEM-EDAX. Those data clearly demonstrated that after ultrasonically controlled HDP of MoO_x

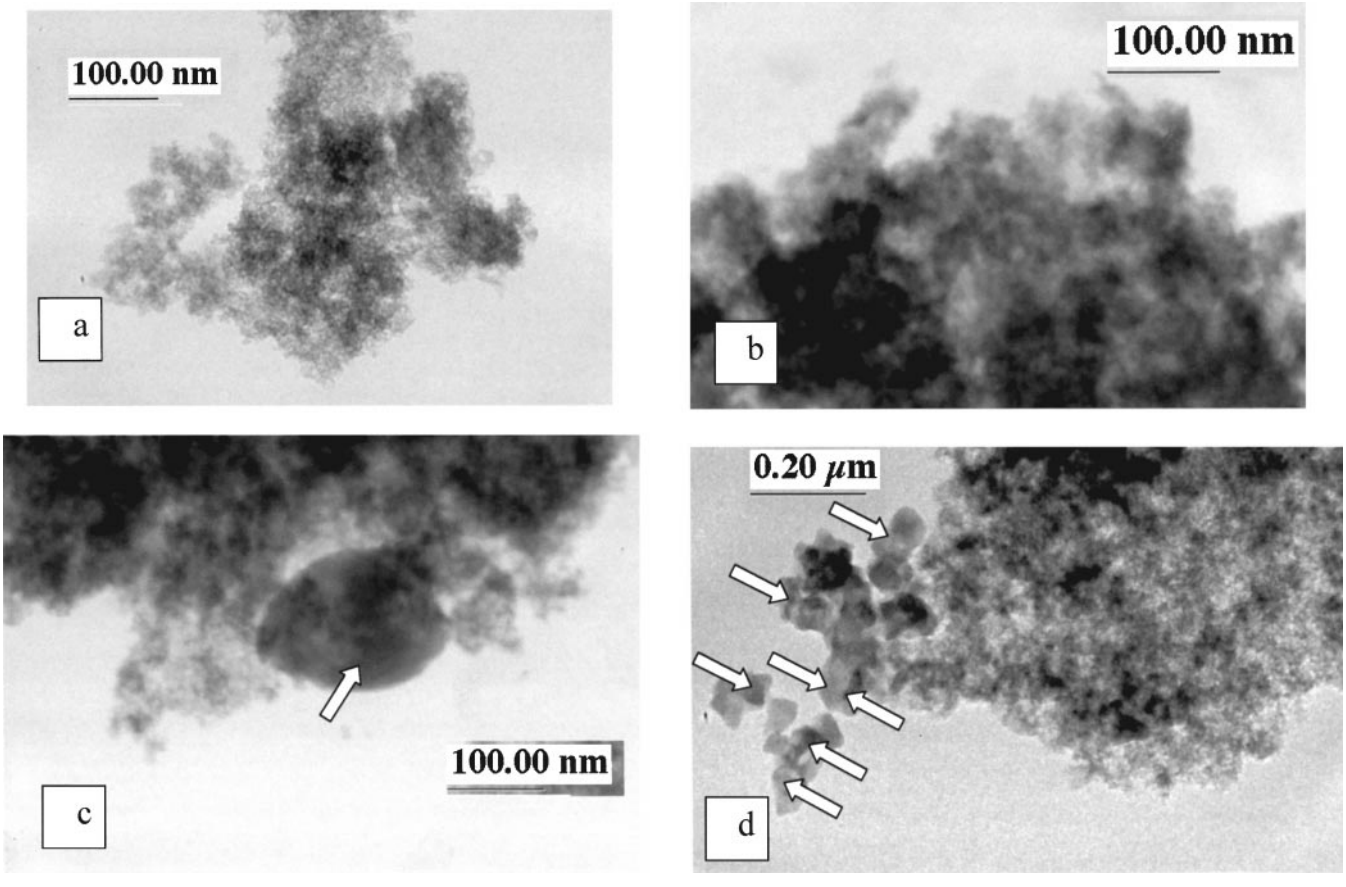

FIG. 8. TEM micrographs of Al-MCM-41 support and MoO_x/Al-MCM-41 composites prepared by ultrasonically controlled HDP: (a) Al-MCM-41; (b) 21% MoO_3/Al-MCM-41; (c) 45% MoO_3/Al-MCM-41; (d) 66% MoO_3/Al-MCM-41.

onto Al-MCM-41 support, the Mo oxide phase is located inside the support pores and does not form separate particles up to a MoO_3 content of about 40–45 wt%. This is a consequence of a very high Mo deposition rate on the Al-MCM-41 surface relative to bulk deposition.

The high-magnification HR-TEM micrographs of pure Al-MCM-41 and MoO_x/Al-MCM-41 composite obtained by ultrasonically controlled HDP with 45 wt% MoO_3 are shown in Fig. 9. Hexagonal pore structure could be detected in both samples. This means that ultrasonically controlled HDP does not cause degradation of the Al-MCM-41 pore structure. The negative image of pure Al-MCM-41 (Fig. 9a) clearly demonstrates the entrances of hexagonal nanotubes forming the pore structure of the support with a wall thickness of ~1.5 nm. Deposition of MoO_x increased the wall thickness to ~2.3 nm (the clearest positive image, Fig. 9b). This is a result of formation of a close-packed monolayer of the MoO_x phase on the surface of Al-MCM-41 pores due to ultrasonically controlled formation of surface Mo silicate species.

It is possible to calculate the theoretical increase of the pore wall thickness by considering a close-packed monolayer of Mo oxide phase and assuming that the density of this phase is equal to the density of Mo blue oxide (3.6 g/cm^3 according to (36)). Simple geometrical consideration of one infinite cylindrical pore leads to a relationship between the Mo oxide loading calculated as MoO_3 weight fraction (y), its density (ρ), the average pore diameters of the parent Al-MCM-41 (D_{MCM}) and MoO_x/Al-MCM-41 ($D_{Mo\text{-}MCM}$), and parent Al-MCM-41 pore volume (PV):

$$D_{MCM}^2\left(1-\frac{y/\rho}{PV(1-y)}\right)=D_{Mo-MCM}^2. \qquad [3]$$

Considering a PV of 1.74 cm^3/g and a 45% MoO_3 loading gives a reduction of average pore diameter of 0.6 nm (from 8.3 to 7.7 nm). This is close to the values measured by HR-TEM (Fig. 9). The thickness of the Mo oxide monolayer on the alumina support was estimated in (37) as 0.3–0.5 nm on the basis of the structural chemistry of MoO_x polyhedra and different alumina planes. It agrees with our HR-TEM data that give a Mo oxide monolayer thickness of $(2.3 - 1.5)/2 = 0.4$ nm.

Theoretical calculations (37, 43) indicate that the close-packed monolayer capacity of any surface is close to 5 Mo atoms/nm^2, based on

- structural chemistry of MoO_x polyhedra and different alumina planes,
- MoO_3 density, and
- effective ionic diameter of MoO_6 octahedra.

This was confirmed by monolayer capacity measurements on alumina (37, 43). Considering the surface area of MCM material used in this work and the Mo surface concentration of 5 Mo atoms/nm^2, the geometrical close-packed monolayer capacity corresponds to a 50% MoO_3 content, which is in good agreement with our measurements.

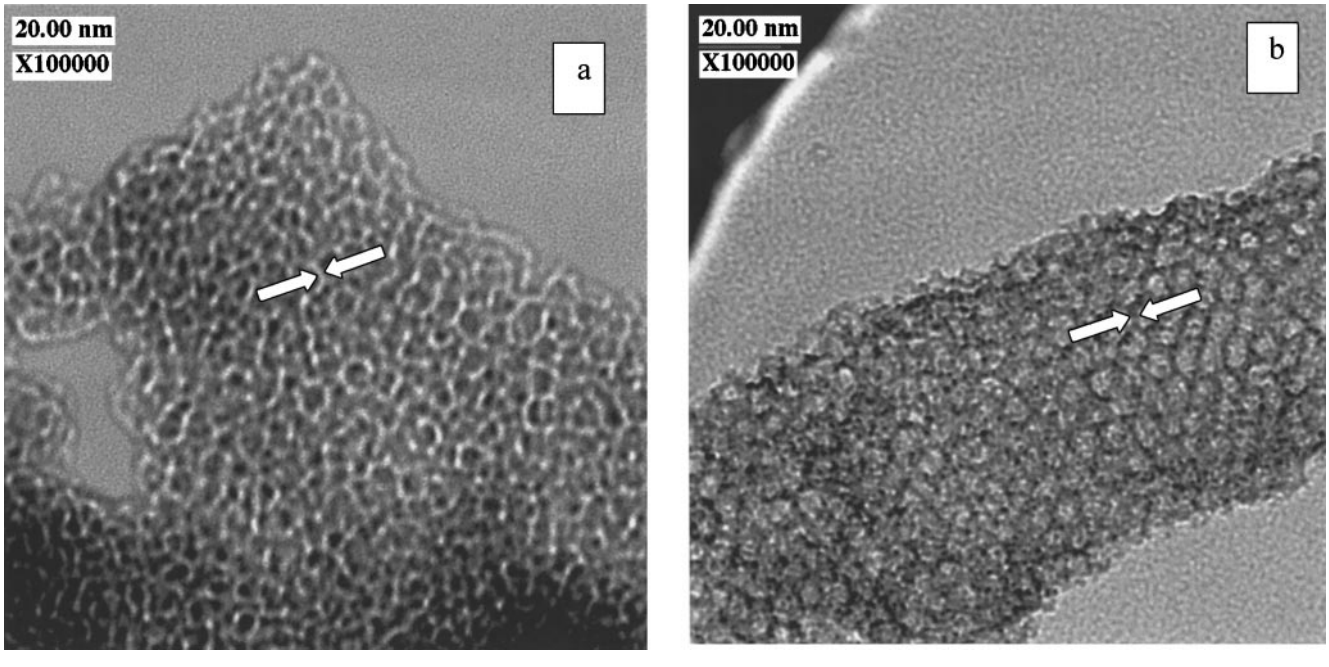

FIG. 9. HR-TEM micrographs of Al-MCM-41 support and MoO_x/Al-MCM-41 composites prepared by ultrasonically controlled HDP: (a) Al-MCM-41; (b) 45% MoO_3/Al-MCM-41.

3.2.2. N_2 adsorption characteristics. Part of the MoO_x phase located inside the Al-MCM-41 pores could form bulk particles blocking the pores. In order to quantify this effect we introduce the concept of normalized surface area (NSA), defined as

$$\mathrm{NSA} = \frac{\mathrm{SA_{catalyst}}}{(1-y)} \frac{1}{\mathrm{SA_{MCM}}}, \qquad [4]$$

where SA is the specific surface area of the parent Al-MCM-41 or the metal oxide/Al-MCM-41 composite, and y is the weight fraction of metal oxides in the catalyst. If the active component is distributed at the support surface in the form of a close-packed monolayer of a given thickness (no pore blocking occurs), the NSA decreases only as a result of narrowing the support pores. For example, for a 45 wt% MoO_3 phase loaded on a wide-pore Al-MCM-41 support, the reduction of pore diameter from 8.3 to 7.7 nm yields a NSA value of 0.93.

The NSA of the Mo (9, 10, 38), Co–Mo (8), Ni (9, 10), and Ni–Mo (7, 9) catalysts deposited on MCM-41 by impregnation and Mo thermal spreading were calculated according to the above equation on the basis of published surface areas of pure supports and corresponding catalysts in oxide form. Those data are presented in Fig. 10a as a function of metals loading together with the NSAs of Mo- and Co–Mo/Al-MCM-41 oxide samples prepared in this study by impregnation and ultrasonically controlled HDP.

Impregnation and thermal spreading yield significant pore blocking, manifested by a linear NSA decrease with increasing metals loading. This is in agreement with the data obtained in (39) by impregnation of silica gel (380 m^2/g) with ammonium heptamolybdate. Even at a low MoO_3 loading of 5 wt%, the catalyst's surface area decreased to 275 m^2/g, corresponding to a NSA value of 0.75. It is well known that MCM materials and silica gels have the same bulk structure as amorphous silica. So, the surface chemical properties should be similar with negative ζ-potential in aqueous solutions. This does not allow adsorption of Mo anions during impregnation. The lack of a chemical interaction (active precursor–support) at the deposition step leads to poor dispersion of the active precursor and blocking of the pores with its large particles.

In contrast, no pore blocking was detected at high values ($\geq$0.87) for catalyst samples prepared with ultrasonically controlled HDP, even at high metal loading up to 60 wt%. The sulfidation needed for conversion of Co–Mo oxide phases into sulfide phases active in HDS could sinter active components and create pore blocking by splitting the $Mo(Co–Mo)O_x$–support chemical bonds formed in the sonication step. The NSA values calculated on the basis of surface areas measured for the parent Al-MCM-41 and sulfided Co-Mo/Al-MCM-41 catalysts prepared by ultrasonication are shown in Fig. 10b. In all cases NSA values of sulfided catalysts prepared by ultrasonically controlled

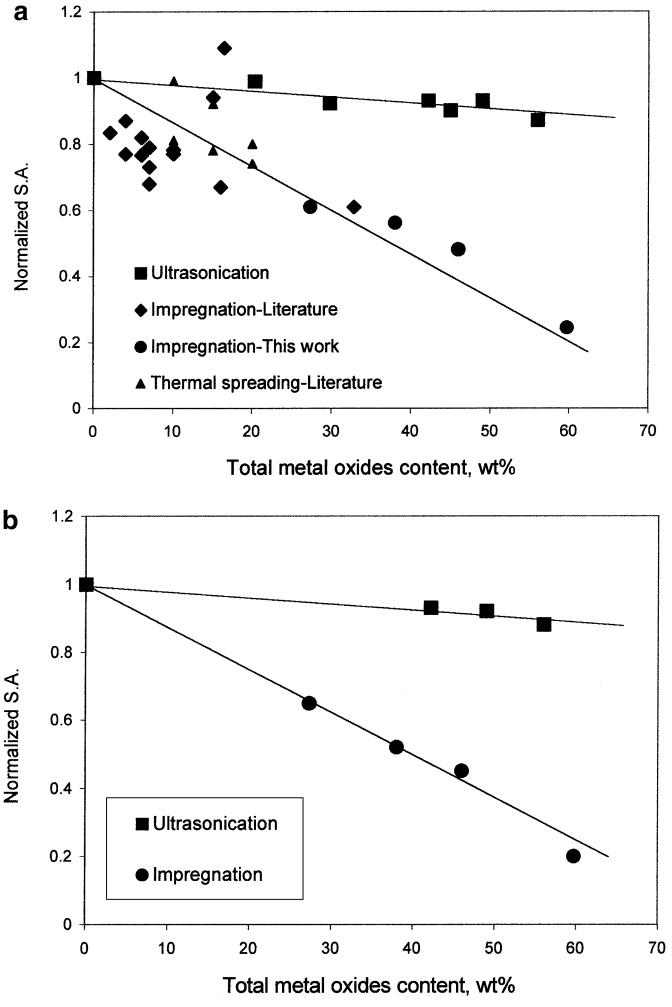

FIG. 10. Normalized surface area of MCM-supported catalysts: (a) Mo–, Ni–, and Co(Ni)–Mo catalysts in oxide form; (b) Co–Mo catalysts after sulfidation.

HDP were equal to or even higher than those of the corresponding oxide precursors, as evidenced for the high thermal stability of a close-packed monolayer of active Co–Mo phases on the Al-MCM-41 surface after sulfidation. The NSA values of impregnated Co–Mo/Al-MCM-41 catalysts after sulfidation were much lower, indicating substantional pore blocking, similar to the case in impregnated oxide catalysts.

The BJH pore size distributions calculated from N_2 desorption isotherms for parent Al-MCM-41 and two oxide Co–Mo/Al-MCM-41 catalysts with close metals loading prepared by impregnation and ultrasonically controlled HDP are shown in Fig. 11. After introduction of Co–Mo oxides by ultrasonication the pore size distribution remains narrow and the pore volume difference ($PV_{support} - PV_{composite}$, cm^3/g) is caused mostly by "dilution" of support with nonporous active components. This is additional evidence for a negligible pore blocking effect. The average pore diameter calculated from the BJH pore size

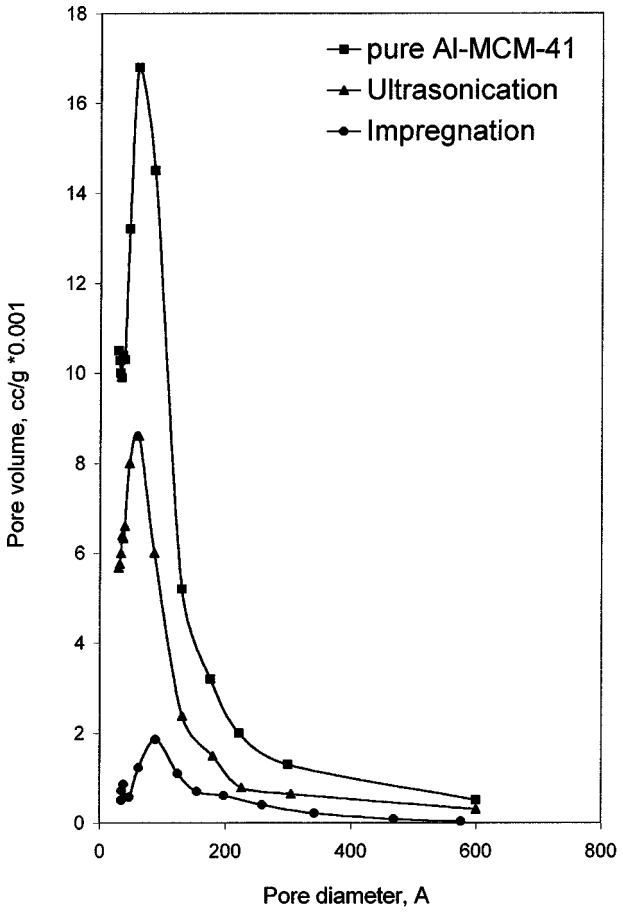

FIG. 11. Pore size distribution of Al-MCM-41 and Co–Mo/Al-MCM-41 catalysts prepared by ultrasonically controlled HDP (13% CoO + 43% MoO_3 or impregnation (13.5% CoO + 46.2% MoO_3).

distribution for the catalyst prepared by ultrasonically controlled HDP decreased by 0.6 nm compared with that of parent Al-MCM-41. This is in good agreement with our HR-TEM data and theoretical calculations. In contrast to ultrasonication, impregnation with the same amount of Co–Mo oxide phases led to a strong decrease of the pore volume much beyond the pore volume difference, caused by "dilution" of support with nonporous active components. In addition, the broadening of the pore size distribution peak for the impregnated sample reflects the formation of bulk particles inside the pores.

3.2.3. XRD characterization of the active phase. Additional information about the location and state of the MoO_x phase in MoO_x/Al-MCM-41 composites was obtained from the XRD patterns of thermally treated samples. As shown by Dhas and Gedanken (18, 19), the Mo blue oxide precipitated from $Mo(CO)_6$ solution under ultrasonication is XRD-amorphous and can be fully crystallized into XRD-crystalline MoO_3 phase by heating in air at 300°C for 48 h. The MoO_x/Al-MCM-41 composites with different Mo loadings prepared by ultrasonically controlled HDP were treated under these conditions after drying. The integral intensity of MoO_3 (020) reflection ($2\theta = 12.8°$) compared with calibration data was used for estimation of the content of the MoO_3 phases in thermally treated samples.

The XRD data are collected in Table 2. At 21 and 45 wt% MoO_3 content a very small fraction (<5%) of MoO_x was crystallized. The location of most of MoO_x inside of support pores in the form of a close-packed monolayer, with chemical bonds MoO_x–support, prevents its crystallization into MoO_3 bulk particles. At a higher Mo loading of 66 wt%, a significant amount of MoO_x phase was crystallized in MoO_3 particles with a domain diameter of 35 nm. Such particles are not located in Al-MCM-41 pores of 6–9 nm but outside, in agreement with TEM data. This means that the crystalline MoO_3 phase could be thermally created only from the MoO_x phase that precipitated outside of the Al-MCM-41 support particles. It confirms the chemical interaction of the MoO_x phase with the support surface in ultrasonically deposited composites and its location inside the support pores up to a MoO_3 loading of 40–45 wt%.

3.2.4. Relative XPS peak intensities. One of the common methods for estimation of the dispersion of Co(Ni)–Mo(W) phases in supported hydrotreating catalysts is determination of the active component/support atomic ratios at the catalyst's surface according to XPS data as a function of active phase content (40–42). This ratio (Me/Al) in supported metal oxide/Al_2O_3 composites increases linearly with a constant slope up to a certain metal loading, where the slope decreases. The first linear part of the curve corresponds to formation of a metal oxide phase monolayer. The point of deviation from linearity indicates full support coverage with a metal oxide phase monolayer. The dependence of the surface Mo/Si ratio on Mo loading was measured by XPS for oxide MoO_x/Al-MCM-41 prepared by ultrasonically controlled HDP. The results are presented in Fig. 12.

The Mo/Si ratio increases linearly with increasing Mo content up to about 40 wt% MoO_3. Further increasing the Mo content caused a drastic rise in the Mo/Si ratio. This unusual behavior of MoO_x deposited on the Al-MCM-41 system could be explained as follows:

TABLE 2

XRD Characterization of Mo/Al-MCM-41 Samples Prepared by Ultrasonically Controlled HDP

		XRD results	
MoO_3 (wt%)	Treatment	Crystallized MoO_3 (wt%)	Average crystal size (nm)
0–100	Without thermal treatment	Amorphous	—
100	300°C for 48 h	100	42.5
21	300°C for 48 h	<1	—
45	300°C for 48 h	<5	—
66	300°C for 48 h	<15	35

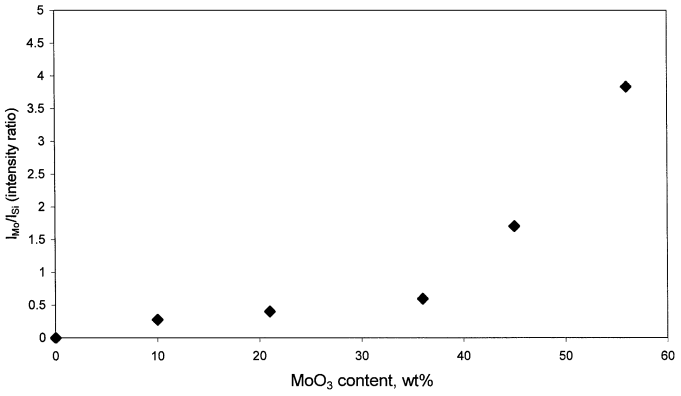

FIG. 12. Surface Mo/Si ratios according to XPS as a function of MoO_x loading in composites prepared by ultrasonically controlled HDP.

- up to ~40 wt% MoO_3 loading on a close-packed monolayer is formed on the walls of Al-MCM-41 pores;
- separate particles of XRD-amorphous Mo blue oxide appear at higher MoO_3 loadings with surface area equal to 115 m^2/g as measured for individual ultrasonically deposited Mo blue oxide.

The high surface area of the separate MoO_x phase formed at high Mo loading and the partial exposure of MoO_x inside the Al-MCM-41 pores to XPS (that collects information from the depth of 3–5 atomic layers due to the shielding effect) are responsible for raising the Mo/Si ratio. Furthermore, the response of MoO_x inside the support pores to XPS depends on the support crystal orientation while that of separate MoO_x particles does not. This causes a strong increase in the relative contribution of Mo atoms to the XPS spectral intensity at high Mo loading. Therefore, the detected dependence of the Mo/Si XPS intensities ratio on Mo loading confirms the formation of a close-packed MoO_x monolayer inside the Al-MCM-41 pores at loading up to 40 wt% MoO_3.

MAS-NMR, TEM, PSD-BET, XRD, and XPS investigations are evidence for formation of a close-packed monolayer of MoO_x phase on the surface of Al-MCM-41 pores due to ultrasonically controlled formation of anchored surface Mo species. The Mo phase deposition rate is about 1 order of magnitude higher in the presence of Al-MCM-41 than in its absence. This is a consequence of an ultrasonically induced chemical interaction between the internal surface of Al-MCM-41 support pores and Mo-containing species (negligible external surface). Therefore, the MoO_x phase is created mostly in the support pores up to 40–45 wt% (TEM, XRD), corresponding to the theoretically calculated full coverage of the Al-MCM-41 surface. The hydrated Mo species in the support pores are highly dispersed, since the concentration of protons near Si atoms increased as a result of Mo phase deposition (MAS-NMR). No MCM pore blocking occurred (NSA $\geq$ 0.87 and PSD) and no crystalline particles were detected inside the pores after thermal treatment (XRD). Furthermore, this MoO_x phase forms a monolayer inside the Al-MCM-41 pores at loading up to 40 wt% MoO_3, linearly increasing the surface Mo/Si atomic ratio (XPS). This corresponds to increasing the support wall thickness (HR-TEM) and decreasing the pore diameter (PSD) by values that fit theoretical calculations. The content of highly dispersed MoO_x phase in the 40–45 wt% MoO_3/Al-MCM-41 composite corresponds to theoretical full coverage of the support's surface, which means that the MoO_x phase forms a close-packed monolayer.

Co phase deposition occurs only on the Al-MCM-41 covered by MoO_x phase. This totally excludes creation of a Co phase outside of the pores (no decomposition of $Co(CO)_3NO$ occurs under the selected conditions in the absence of Mo-covered MCM) and implies high dispersion of Co species over a close-packed monolayer of MoO_x phase. Co-phase high dispersion only inside the pores was confirmed by TEM (no separate Co-containing particles were detected), XRD (no Co-containing crystalline phase was detected in thermally treated Co-Mo/Al-MCM-41 samples), and N_2 adsorption (NSA $\geq$ 0.87).

3.3. Catalysts' HDS Performance

Assuming that catalysts with maximum Mo loading corresponding to monolayer coverage should display the highest HDS activity, Mo contents in the ultrasonically deposited sample MoO_x/Al-MCM-41 in the range of 40–50 wt% MoO_3 were selected for testing the effect of the Co/Mo ratio on the DBT HDS rate. Different amounts of Co and Mo oxide were deposited onto Al-MCM-41 by two-step ultrasonically controlled HDP, so that at fixed Mo content (43 wt% MoO_3) the Co/(Co + Mo) ratio varied from 0 to 0.36. The effect of the Co/(Co + Mo) ratio on the activity measured after catalyst sulfidation is shown in Fig. 13. Increasing the Co content in the catalyst increased the

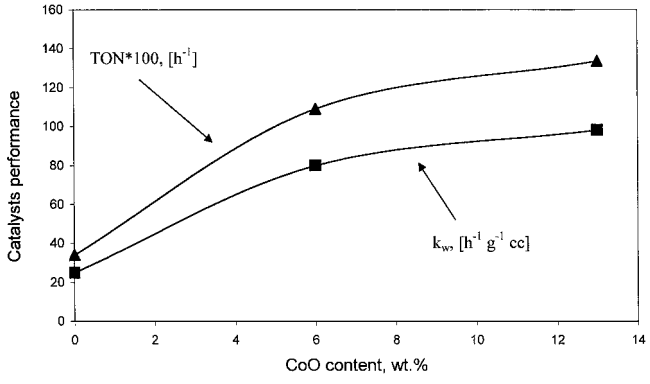

FIG. 13. Performance of Co–Mo/Al-MCM-41 catalysts prepared by ultrasonically controlled HDP in dibenzothiophene HDS (43 wt% MoO_3 and different CoO contents).

TABLE 3

Comparison of Catalysts' Performance in Hydrodesulfurization of DBT

Catalyst	Deposition method	S.A. (m^2/g)	P.V. (cm^3/g)	NSA	CoO (wt%)	MoO_3 (wt%)	k_w ($h^{-1}\,g^{-1}\,cm^3$)	TON (h^{-1})
Co–Mo/γ-Al_2O_3 commercial catalyst	Unknown	220	0.45	—	5.7	26.5	57	1.26
Co–Mo/γ-Al_2O_3	Impregnation	200	0.43	1.03	5.7	22.1	63	1.67
Co–Mo/γ-Al_2O_3	Impregnation	60	0.19	0.52	12.0	45.0	24	0.31
Co–Mo/γ-Al_2O_3	Ultrasonication	190	0.45	0.98	5.8	22.2	67	1.77
Co–Mo/Al-MCM-41	Impregnation	360	0.44	0.59	5.2	22.1	22	0.58
Co–Mo/Al-MCM-41	Impregnation	82	0.31	0.24	13.5	46.2	55	0.69
Co–Mo/Al-MCM-41	Ultrasonication	450	0.90	0.93	9.5	32.7	81	1.45
Co–Mo/Al-MCM-41	Ultrasonication	320	0.63	0.87	13.0	43.0	98	1.34

total catalyst activity and the specific activity of active phase (TON). Both reached a maximum value at a Co/(Co + Mo) ratio of about 0.3, corresponding to the well-known Co–Mo promotion effect observed in many Co–Mo sulfide systems (27, 28). This result indicates that the nature of the Co–Mo sulfide phase in Co–Mo/Al-MCM-41 catalysts prepared by ultrasonication is close to that in the catalysts prepared by conventional methods and implies that the Co phase is well dispersed over Mo-covered Al-MCM-41.

Table 3 presents the HDS performance of a series of Co–Mo catalysts deposited on Al-MCM-41 by different methods at different Co–Mo loadings compared with Co–Mo catalysts deposited on commercial γ-Al_2O_3 and with commercial Co–Mo–Al catalyst.

The activities of commercial Co–Mo–Al and catalysts on γ-Al_2O_3 prepared by impregnation or ultrasonically controlled HDP at 5.7–5.8 wt% CoO–22.1–26.5 wt% MoO_3 loading were similar. This reflects the similar nature and dispersion of active sulfide Co–Mo–S phase in these catalysts. Increasing the Co–Mo loading at optimal Co/(Co–Mo) ratio in Co–Mo–Al catalyst prepared by impregnation up to 12.0 wt% CoO and 45.0 wt% MoO_3 decreased strongly the catalyst's activity. Furthermore, it decreased the HDS TON due to substantial blocking of support pores (NSA = 0.52). That corresponds to a decrease in the catalyst surface area from 200 to 60 m^2/g. Thus, the potential HDS activity of a Co–Mo catalyst on alumina supports (as well as a commercial Co–Mo–Al catalyst) is limited by their capacity to accommodate a monolayer coverage of active components. This capacity is up to about 6 wt% CoO and 25 wt% MoO_3. This correlates very well with theoretical full close-packed MoO_3 monolayer capacity estimated on the basis of 5 Mo atoms/nm^2 and a γ-alumina specific surface area of 270 m^2/g.

The HDS activity of a Co–Mo/Al-MCM-41 catalyst prepared by impregnation (5.2 wt% CoO–22.1 wt% MoO_3) was about 2.5 times lower than the activity of Co–Mo–Al catalysts at the same Co–Mo loading. This could be explained by invoking substantial pore blocking of the Al-MCM-41 support (NSA = 0.59), so that part of the active phase was inaccessible for reacting DBT molecules. Increasing the Co–Mo loading to 13.5 wt% CoO–46.2 wt% MoO_3 in impregnated Co–Mo/Al-MCM-41 catalyst significantly increased its HDS activity (k_w) at slightly increased TON due to progressive pore blocking (NSA = 0.24). The Co–Mo–Al catalyst displayed a significant drop in activity (both k_w and TON) at this loading level.

Ultrasonically controlled HDP of Co–Mo components on Al-MCM-41 avoided pore blocking. At both Co–Mo loadings the NSA was close to 0.9. Therefore, the TON values in both cases were high and similar to that measured with commercial Co–Mo–Al catalysts. As a result, the activity of the Co–Mo/Al-MCM-41 catalysts prepared by ultrasonically controlled HDP (k_w) was 30–55% higher than that of the Co–Mo–Al catalysts, depending on Co–Mo loading. Those results demonstrate the capability of Al-MCM-41 supports to provide a higher capacity of the MoO_x monolayer compared with commercial γ-Al_2O_3 or random pore structure silica gel. Apparently, the pore structure engineering of MCM-41 does not influence the Co–Mo–S phase structure and catalytic activity. Ultrasonically controlled HDP of Co–Mo components is the only reported method that takes full advantage of the MCM-41 support. As a result, fully covered Al-MCM-41-supported catalyst, prepared by ultrasonically controlled HDP, contained much more active phase (13 wt% CoO–43 wt% MoO_3) and displayed 1.7 times higher activity in HDS of DBT (k_w) compared with fully covered γ-alumina-supported catalyst (5.7 wt% CoO–22.1 wt% MoO_3).

4. CONCLUSION

Ultrasonication of a slurry containing a metal carbonyl and a high-surface-area silica-based mesoporous material (Al-MCM-41) yielded, for the first time, deposition–precipitation of the corresponding metal oxide, forming a close-packed monolayer on the surface. Deposition–precipitation of Mo and Co oxides and their fixation at the

surface of Al-MCM-41 in the form of a monolayer is a result of an ultrasonically induced chemical interaction between metal carbonyl (oxide) and the surface silica atomic layer, yielding surface silicates. This interaction increases the Mo oxide deposition rate at the support's surface by an order of magnitude compared with that of bulk precipitation. This study demonstrated that complete monolayer coverage of a wide-pore Al-MCM-41 surface, corresponding to ~45 wt% MoO_3 loading, could be achieved by ultrasonically controlled deposition–precipitation. This high-loading Co–Mo/Al-MCM-41 catalyst was 1.7 times more active in HDS of dibenzothiophene than commercial Co–Mo–Al catalyst.

ACKNOWLEDGMENTS

We acknowledge the financial support of the Israeli Ministry of Science. This research was supported in part by the Israel Science Foundation founded by the Israel Academy of Science & Humanities. We also thank Prof. S. Vega and Dr. S. Kababya for conducting the MAS NMR measurements and for useful discussions.

REFERENCES

1. Beck, J. S., Vartuli, J. C., Roth, W. J., Leonowicz, M. E., Kresge, C. T., Schmitt, K. D., Olson, D. H., Sheppard, E. W., McCullen, S. B., Higgins, J. B., and Schlenker, J. L., *J. Am. Chem. Soc.* **114** (27), 10834 (1992).
2. Corma, A., *Chem. Rev.* **97** (6), 2373 (1997).
3. Benesi, H. A., Curtis, R. M., Studer, H. P., *J. Catal.* **10**, 328 (1968).
4. Yang, Y., Pan, J., Zheng, N., Liu, X., and Zhang, J., *Appl. Catal.* **61**, 75 (1990).
5. Hadjiivanov, K., Mihaylov, M., Klissurski, D., Stefanov, P., Abadjieva, N., Vassileva, E., and Mintchev, L., *J. Catal.* **185**, 314 (1999).
6. Jozwiak, W. K., and Lana, I. G. D., *J. Chem. Soc., Faraday Trans.* **93** (15), 2583 (1997).
7. Corma, A., Martinez, A., Martinez-Soria, V., and Monton, J. B., *J. Catal.* **153**, 25 (1995).
8. Song, C., andReddy, K. M., *Appl. Catal. A* **176**, 1 (1999).
9. Yue, Y., Sun, Y., and Gao, Z., *Catal. Lett.* **47**, 167 (1997).
10. Cui, J., Yue, Y., Sun, Y., and Gao, Z., *Stud. Surf. Sci. Catal.* **105**, 687 (1997).
11. Yermakov, Yu. I., Startev, A. N., and Burmistrov, V. A., *Appl. Catal.* **11**, 1 (1984).
12. Zaikovskii, V. I., Plyasova, L. M., Burmistrov, V. A., Startev, A. N., and Yermakov, Yu. I., *Appl. Catal.* **11**, 15 (1984).
13. Rahiala, H., Beurroies, I., Eklund, T., Hakala, K., Gougeon, R., Trens, P., and Rosenholm, J. B., *J. Catal.* **188**, 14 (1999).
14. Hermans, L. A. M., and Geus, J. W., *Stud. Surf. Sci. Catal.* **3**, 113 (1979).
15. Geus, J. W., and van Dillen, A. J., *in* "Preparation of Solid Catalysts" (G. Ertl, H. Knozinger, and J. Weitkamp, Eds.), p. 460. Wiley-VCH, Weinheim, 1999.
16. van Stiphout, P. C. M., Donker, H., Bayense, C. R., and Geus, J. W., *Stud. Surf. Sci. Catal.* **31**, 55 (1987).
17. de Jong, K. P., and Geus, J. W., *Appl. Catal.* **4**, 41 (1982).
18. Dhas, N. A., and Gedanken, A., *J. Phys. Chem. B* **101**, 9495 (1997).
19. Dhas, N. A., and Gedanken, A., *Chem. Mater.* **9**, 3144 (1997).
20. Jeevanandam, P., Koltypin, Y., Gedanken, A., and Mastai, Y., *J. Mater. Chem.* **10** (2), 511 (2000).
21. Helnerman, J. J. L., van Hengstum, A. J., and de Wind, M., Eur. Patent Appl. 0469675 Al, 1991.
22. Wagner, C. D., Davis, L. E., Zeller, M. V., Taylor, J. A., Raymond, R. H., and Gale, L. H., *Surf. Interface Anal.* **3**, 211 (1981).
23. Evans, S., *Surf. Interface Anal.* **17**, 85 (1991).
24. Landau, M. V., Herskowitz, M., Givoni, D., Laichter, S., and Yitzhaki, D., *Fuel* **77**, 3 (1998).
25. Broderick, D. H., and Gates, B. C., *AIChE J.* **27** (4), 663 (1981).
26. Singhal, G. H., Espino, R. L., Sobel, J. E., and Huff, G. A., *J. Catal.* **67**, 457 (1981).
27. Topsoe, H., Clausen, B. S., and Massoth, F. E., *in* "Hydrotreating Catalysis" (J. R. Anderson and M. Boudart, Eds.). Springer, Berlin, 1996.
28. Whitehurst, D. D., Isoda, T., and Mochida, I., *Adv. Catal.* **42**, 345 (1998).
29. Briggs, D., and Sean, M. P., "Practical Surface Analysis", 2nd Ed., Vol. 1. Wiley, New York, 1990.
30. Suslick, K. S., and Price, G. J., *Annu. Rev. Mater. Sci.* **29**, 295 (1999).
31. Leighton, T. G., "The Acoustic Bubble." Academic Press, London, 1994.
32. Mestl, G., and Srinivasan, T. K. K., *Catal. Rev.-Sci. Eng.* **40**, 451 (1998).
33. Braun, S., Appel, L. G., Camorim, V. L., and Schmal, M., *J. Phys. Chem. B* **104**, 6584 (2000).
34. Piquemal, J. Y., Manoli, J. M., Beaunier, P., Ensuque, A., Tougne, P., Legrand, A. P., and Bregeault, J. M., *Microporous Mesoporous Mater.* **29**, 291 (1999).
35. Landau, M. V., Varkey, S. P., Herskowitz, M., Regev O., Pevzner, S., Sen, T., and Luz, Z., *Microporous Mesoporous Mater.* **33**, 149 (1999).
36. Weast, R. C., and Astle, M. J., "CRC Handbook of Chemistry and Physics," 62nd Ed., p. B-121. CRS Press, New York, 1982.
37. Sonnemans, J., and Mars, P., *J. Catal.* **31**, 209 (1973).
38. Ookoshi, T., and Onaka, M., *Chem. Commun.* **1998**, 2399.
39. Hu, H., Wachs, I. E., and Bare, S. R., *J. Phys. Chem.* **99**, 10897 (1995).
40. Okamoto, Y., and Imanaka, T., *J. Phys. Chem.* **92**, 7102 (1988).
41. Imamura, S., Sasaki, H., Shono, M., and Kanai, H., *J. Catal.* **177**, 72 (1998).
42. Wang, X., Zhao, B., Jiang, D., and Xie, Y., *Appl. Catal. A* **188**, 201 (1999).
43. Hillerova, E., Morishige, H., Inamura, K., and Zdrazil, M., *Appl. Catal. A* **156**, 1 (1997), and references therein.